



# Crosslinked perfluoropolyether solid electrolytes for lithium ion transport



Didier Devaux<sup>a,b,c</sup>, Irune Villaluenga<sup>a,b,c</sup>, Mahesh Bhatt<sup>b,c,d</sup>, Deep Shah<sup>c</sup>, X. Chelsea Chen<sup>d</sup>,  
Jacob L. Thelen<sup>b,c,d</sup>, Joseph M. DeSimone<sup>e,f</sup>, Nitash P. Balsara<sup>a,b,c,d,\*</sup>

<sup>a</sup> Environmental Energy Technologies Division, Lawrence Berkeley National Laboratory, Berkeley, CA 94720, USA

<sup>b</sup> Joint Center for Energy Storage Research (JCESR), Lawrence Berkeley National Laboratory, Berkeley, CA 94720, USA

<sup>c</sup> Department of Chemical and Biomolecular Engineering, University of California, Berkeley, CA 94720, USA

<sup>d</sup> Materials Science Division, Lawrence Berkeley National Laboratory, Berkeley, CA 94720, USA

<sup>e</sup> Department of Chemistry, University of North Carolina at Chapel Hill, Chapel Hill, NC 27599-3290, USA

<sup>f</sup> Department of Chemical and Biomolecular Engineering, North Carolina State University, Raleigh, NC 27695, USA

## ARTICLE INFO

### Keywords:

Perfluoropolyether  
Polyhedral oligomeric silsesquioxane  
Solid electrolyte  
Crosslinked electrolyte  
Lithium battery

## ABSTRACT

Perfluoropolyethers (PFPE) are commercially available non-flammable short chain polymeric liquids. End-functionalized PFPE chains solvate lithium bis(trifluoromethanesulfonyl)imide (LiTFSI) salt and these mixtures can be used as electrolytes for lithium (Li) batteries. Here we synthesize and characterize a new class of solid PFPE electrolytes. The electrolytes are made by either thermal or UV crosslinking PFPE chains with urethane methacrylate end-groups. For the synthesis of thermally crosslinked electrolytes, polyhedral oligomeric silsesquioxane (POSS) with organic acrylopropyl groups was used as crosslinker agent, while for UV cured electrolytes a photoinitiator was used. We present thermal, morphological, and electrical data of the solid electrolytes. We compare these properties with those of the two parent liquids (PFPE with urethane methacrylate end-groups and POSS with acrylopropyl groups) mixed with LiTFSI. The solubility limit of LiTFSI in the PFPE-based solids is higher than that in the liquids. The conductivity data are analyzed using the Vogel–Tamman–Fulcher equation. The concentration of effective charge carriers is a strong function of the nature of the solvent (solid versus liquid) whereas the activation energy is neither a strong function of the nature of the solvent nor salt concentration.

## 1. Introduction

Solid polymer electrolytes are one of the key materials that could lead to the development of next generation rechargeable lithium (Li) batteries [1,2]. Poly(ethylene oxide) (PEO) laden with alkali metal salt is the most studied polymer electrolyte since the initial works by Fenton et al. and Armand et al. [3,4]. A commonly used salt is lithium bis(trifluoromethanesulfonyl)imide (LiTFSI). The performance of electrolytes depends on many parameters such as ionic conductivity, cation transference number, salt diffusion coefficient, and the thermodynamic factor [5,6]. For practical applications, the ionic conductivity of electrolytes must exceed  $10^{-5}$  S/cm; one may consider this to be the lower limit for a viable electrolyte regardless of the values of the other transport and thermodynamic factors. The requisite conductivity in PEO electrolytes is only obtained in the rubbery state, above the PEO melting temperature, which is in the vicinity of 60 °C. At this temperature, conductivities as high as  $10^{-3}$  S/cm are obtained [7,8]. Unfortunately, in this state, PEO is a viscoelastic liquid; in order to create solids, one must chemically crosslink the PEO chains.

Numerous polyether-based crosslinked polymer electrolytes have been studied [9–18]. Simple strategies for crosslinking usually involve thermally activated reactions or UV irradiation [18–21]. Unfortunately, the ionic conductivity of these solids is often below  $10^{-5}$  S/cm at room temperature [22]. In an important study, Pan et al. developed a series of crosslinked polymer electrolytes using PEO as the conducting polymer and polyhedral oligomeric silsesquioxane (POSS) as the crosslinker [19]. Through a one-step thermally activated reaction between octakis(3-glycidioxypropyl)dimethylsiloxy)octasilsesquioxane (octa-POSS) and amine-terminated PEO in the presence of LiTFSI, electrolytes with ionic conductivity higher than  $10^{-5}$  S/cm at 30 °C, and close to  $10^{-3}$  S/cm at 90 °C, were produced. These values are very similar to that of PEO homopolymer doped with LiTFSI [23]. It is perhaps surprising that in this particular system, crosslinking does not hinder ion transport.

Functionalized POSS particles are ideally suited for fundamental studies due to their well-defined organic/inorganic architecture at the molecular level and the wide range of organic outer shells that can be attached to the POSS particles [24–26]. Wunder and coworkers

\* Corresponding author at: Department of Chemical Engineering, 201 Gilman Hall, University of California, Berkeley, CA 94720-1462, USA.  
E-mail address: [nbalsara@berkeley.edu](mailto:nbalsara@berkeley.edu) (N.P. Balsara).

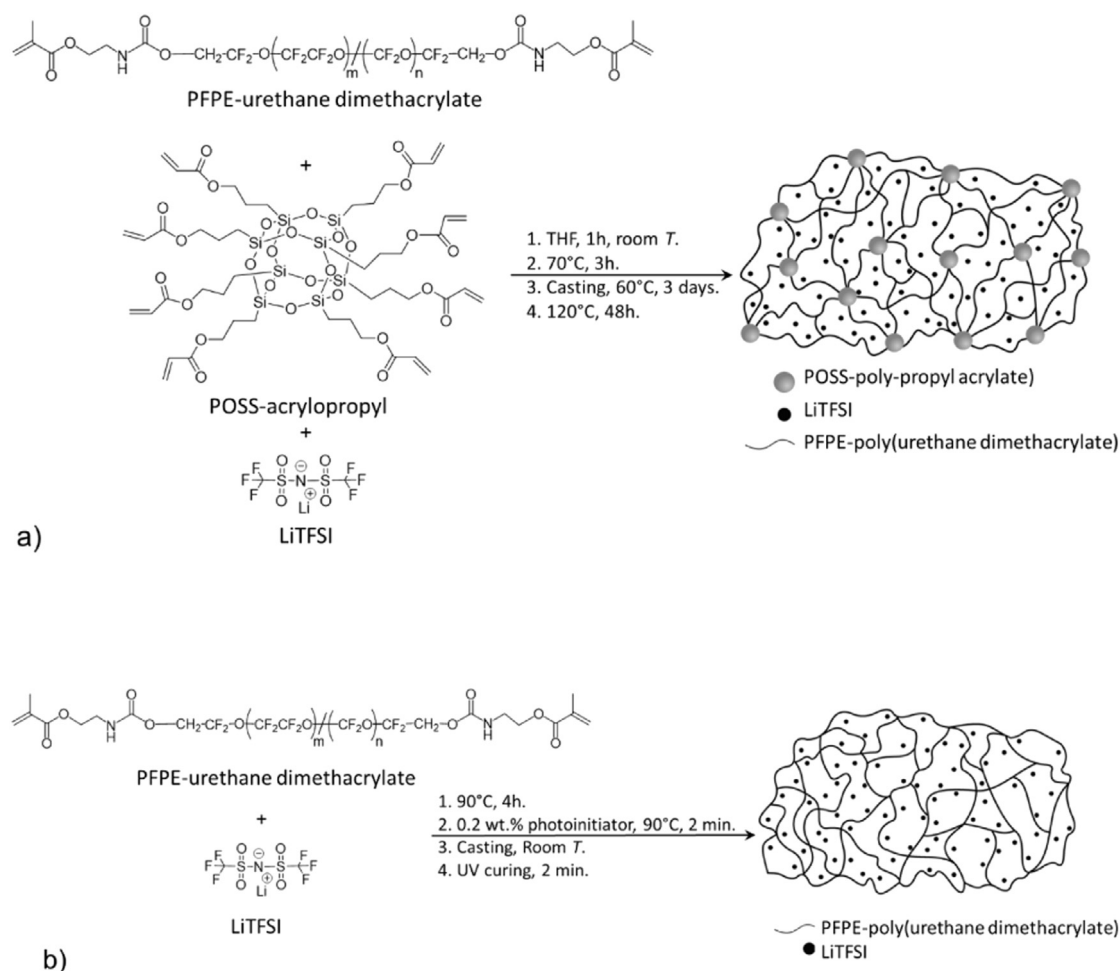


Fig. 1. Schematic of the reactions to produce (a) thermally and (b) UV crosslinked electrolytes.

investigated PEO-terminated POSS as a liquid based electrolyte depending on the PEO chain length and the Li salt nature [27–31]. For short PEO chains, between 4 and 8 repeat units, the ionic conductivity at room temperature is about  $10^{-4}$  S/cm. Another electrolyte, developed by the same group, comprised of a mixture of PEO and functionalized Li salt based on multi-ionic POSS had a room temperature ionic conductivity similar to the PEO-terminated POSS electrolyte [32]. In the context of polymer electrolytes, the inorganic POSS content is usually considered as a minor non-ionically-conductive component. There is considerable controversy surrounding the effect of inorganic oxides on the conductivity of PEO/inorganic hybrid electrolytes. In early work, it was thought that the addition of inorganic fillers such as silica and alumina (particle sizes in the sub-micron to micron range) could enhance the conductivity of rubbery electrolytes by factors as large as 200 due to interactions between the polymer, salt, and filler that are generally referred to as “space-charge” effects [33]. More recent studies, however, suggest that the addition of fillers can lead to a decrease in the conductivity of rubbery electrolytes. Efforts to study polymer-salt-filler interactions by spectroscopy have led to the conclusion that “space-charge” effects are absent [34].

Conventional ether- and carbonate-based electrolytes dissolve salts due to interactions between the cation and oxygens in the electrolyte that are characterized by a partial negative charge. To our knowledge, all of the solid polymer electrolytes studied thus far fall into this category. In the rubbery state, ion transport is coupled to segmental motion, which, in turn is coupled to the glass transition temperature ( $T_g$ ). One of the limitations of PEO-based electrolytes is the rapid increase in  $T_g$  with added salt due to the interactions between oxygen-bearing segments

and lithium cations [8,35]. While the  $T_g$  of pure PEO is in the vicinity of  $-65^\circ\text{C}$ , that of PEO electrolytes with optimal lithium salt concentration is in the vicinity of  $-45^\circ\text{C}$  [8,36]. In recent work, we examined the possibility of using mixtures of lithium salts and perfluoropolyethers (PFPEs) as electrolytes for lithium batteries [37–41]. Perfluoropolyethers are non-crystalline, non-flammable short chain polymers with extremely low  $T_g$ ; the  $T_g$  of pure PFPEs is in the vicinity of  $-90^\circ\text{C}$ . Preliminary evidence suggests that the ability of PFPE-based electrolytes to dissolve salts is due to interactions between the fluorinated anions in the salt and the fluorinated backbones of PFPE [37]. To date, all of the published work on PFPE electrolytes is limited to liquid electrolytes.

The purpose of this paper is to report on the synthesis and characterization of solid PFPE electrolytes with LiTFSI. We present data on two types of crosslinked PFPEs: thermally crosslinked POSS-based PFPE electrolytes inspired by Pan et al. [19] and UV crosslinked solids inspired by the work of Williams et al. [42]. The POSS-based system was obtained by reacting acrylate-functionalized POSS with PFPE. We show that crosslinking increases the solubility of LiTFSI in PFPE-based solids (both POSS and UV crosslinked systems). Our data suggest that POSS particles may play an important role in ion transport; mixtures of acrylate-functionalized POSS and LiTFSI exhibit significant conductivity. The conductivities of solid PFPE electrolytes can be as high as  $10^{-4}$  S/cm at elevated temperatures. In future work, we hope to measure other transport and thermodynamic properties of these solid electrolytes.

## 2. Experimental section

### 2.1. Materials

Perfluoropolyether-urethane methacrylate (Fluorolink® MD700, Solvay) (PFPE) was purchased from the supplier Cornerstone Technology Inc. The PFPE average molecular weight from the material datasheet is 1920 g/mol. Polyhedral oligomeric silsesquioxane with organic acrylopropyl groups attached at the corners of the POSS cage, with a formula weight of 1321.75 g/mol, was purchased from Hybrid Plastic Inc. (Acrylo POSS MA0736,  $(C_6H_9O_2)_n(SiO_{1.5})_n$ ) (POSS). The  $\alpha$ -hydroxycyclohexyl phenylketone photoinitiator and inhibitor-free anhydrous tetrahydrofuran (THF) solvent were obtained from Sigma Aldrich. All materials were stored and used as received in an argon filled MBraun glovebox with ultralow concentrations of water and oxygen. Prior to use, lithium bis(trifluoromethanesulfonyl)imide (LiTFSI) obtained from Novolyte was dried at 120 °C under vacuum for three days in the glove box antechamber before being brought inside the glove box.

### 2.2. Electrolytes formulation

All the liquid- and solid-based electrolytes were prepared inside an argon glove box. Liquid-based electrolytes were formulated by mixing PFPE, or POSS, with a predetermined amount of LiTFSI at 90 °C until complete dissolution of the salt was observed by the naked eye. Typical mixing times were in the range of 4 h. The LiTFSI weight fraction ( $w_{LiTFSI}$ ) in PFPE- and POSS-based liquid electrolyte was varied between 0 and 0.50. The PFPE- and POSS-based liquid electrolytes are labelled PFPE- $w_{LiTFSI}$  and POSS- $w_{LiTFSI}$ , respectively.

Our approach for synthesizing thermally crosslinked solid electrolytes is summarized in Fig. 1a. POSS, PFPE, and LiTFSI were first dissolved in THF and stirred for 1 h at room temperature followed by 3 h at 70 °C. The solution was cast on a polytetrafluoroethylene (PTFE) Petri dish and dried at 60 °C for 3 days to ensure complete solvent evaporation. Dry solid electrolytes were obtained by annealing the cast films inside the glove box antechamber for 48 h under vacuum at 120 °C. During this step, the PFPE methacrylate end groups react with the acrylate groups on the POSS molecules to generate a crosslinked network. After cooling down to room temperature, the resulting electrolyte films were peeled off the Petri dish. These crosslinked electrolytes are labelled XL-POSS $w_{POSS}$ -PFPE- $w_{LiTFSI}$ , with  $w_{POSS}$  and  $w_{LiTFSI}$  the weight fraction of POSS and LiTFSI, respectively. The weight fraction of POSS was varied between 0.24 and 0.49, while  $w_{LiTFSI}$  was varied between 0 and 0.52.

Solid electrolytes were also obtained by a UV activated crosslinked reaction as summarized in Fig. 1b. PFPE and LiTFSI were mixed together at 90 °C until complete dissolution of the salt, as seen by the naked eye, typically for 4 h. Then, 0.2 wt% of photoinitiator was added to the mixture and stirred for 2 min at 90 °C. The final mixture was cast on a PTFE Petri dish at room temperature. A solid film was obtained by a UV irradiation step inside the glove box using light with a wavelength of 365 nm (UV curing chamber ELC-500, Electron-Lite Co.) for 2 min. The UV activated crosslinked electrolytes are labelled XL-PFPE- $w_{LiTFSI}$ , with  $w_{LiTFSI}$  ranging in between 0 and 0.5.

### 2.3. Thermal characterization

The thermal properties of the electrolytes were studied by differential scanning calorimetry (DSC). Inside the argon glove box, electrolyte samples were sealed in aluminum (Al) hermetic pans and DSC experiments were performed on a TA Instruments DSC Q200 instrument. The samples were first equilibrated at -90 °C, and two heating-cooling cycles were performed in between -90 and 150 °C at 10 °C/min. The electrolyte glass transition temperatures ( $T_g$ ) were extracted from the second heating cycle.

Thermogravimetric analysis (TGA) was carried out to determine the solid electrolyte thermal stability. The samples, placed in an Al pan, were equilibrated at 40 °C, and heated up to 600 °C at 10 °C/min under a constant flow of argon gas. For comparison, the LiTFSI salt was also characterized, starting at 140 °C. The onset temperature of electrolyte degradation ( $T_d$ ) corresponds to a 5% weight loss.

### 2.4. Symmetric cell assembly and characterization

Stainless-steel symmetric cells were assembled inside the argon glove box. The liquid-based electrolytes filled a 0.3 cm diameter hole of a 254  $\mu$ m-thick silicone spacer that defines the active area ( $S$ ) of the cell. Two 200  $\mu$ m-thick stainless steel blocking electrodes were then placed on each side of the electrolyte-spacer assembly and pressed at room temperature. At each step of the assembly the overall thickness was measured to monitor the electrolyte thickness ( $l$ ). An Al tab was taped on each stainless steel electrode and the assembly was vacuum sealed in a pouch bag (Showa Denko). For the solid electrolytes a similar cell assembly was used except that a wider electrolyte disk than the stainless-steel electrode diameter was punched from the dry electrolyte film. The active cell area,  $S$ , was defined by the stainless steel electrodes which were 1.5 cm in diameter.

The cells were mounted into a custom heating stage and connected to a potentiostat (VMP3, Bio-Logic SAS). Impedance spectroscopy experiments were performed using an ac voltage between 10 and 40 mV in a frequency range between  $10^6$  and 1 Hz. The temperature ( $T$ ) program consisted of an initial heating scan from 30 to 90 °C in 10 °C steps, followed by cooling scan to 30 °C using 10 °C steps. This was followed by a second heating scan similar to the first one. The data were analyzed from the cooling scan and subsequent heating scan. A typical impedance spectrum of the XL-POSS $_{0.12}$ -PFPE $_{0.3}$  electrolyte at 90 °C is shown in Fig. 2. For each  $T$ , the equilibrated value of  $R_{el}$  was extracted from the impedance spectra by fitting the profile with an equivalent electrical circuit consisting of inductance, resistors and constant phase elements [23]. This circuit, shown in the inset of Fig. 2, is composed of the apparatus resistance ( $R_c$ ) and inductance ( $L_c$ ), in series with  $R_{el}$  in parallel with the electrolyte pseudo-capacitance ( $CPE_{el}$ ), in series with the blocking electrode electrolyte interface pseudo-capacitance ( $CPE_{int}$ ). After the experiments, the cells were returned to the argon glove box and disassembled to determine the final electrolyte thickness,  $l$ . Conductivity,  $\sigma$ , at a given temperature,  $T$ , was calculated using Eq.

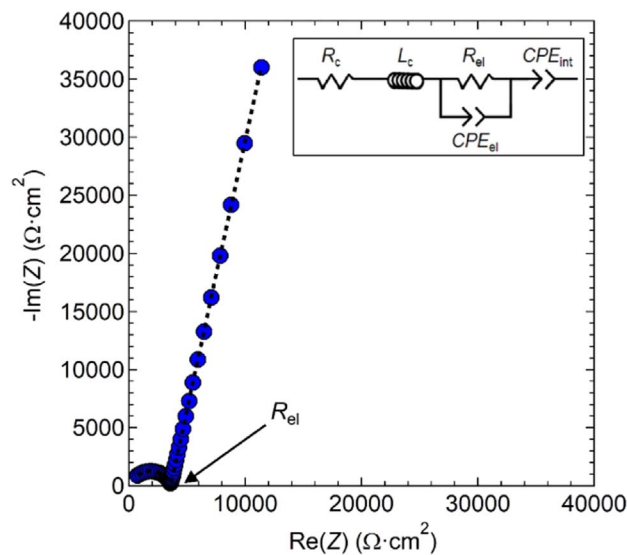


Fig. 2. AC impedance spectrum at 90 °C of the XL-POSS $_{0.12}$ PFPE $_{0.3}$  electrolyte. The symbols are the experimental data and the dashed line corresponds to the best fit using the electrical equivalent circuit shown in the inset.

(1):

$$\sigma(T) = \frac{l}{S \cdot R_{el}(T)} \quad (1)$$

The average conductivity for each electrolyte was determined from three to five independent measurements and the error bars represent the standard deviation.

### 2.5. Morphology characterization

The morphologies of two representative solid electrolytes, XL-PFPE<sub>0.40</sub> and XL-POSS<sub>0.13</sub>PFPE<sub>0.35</sub>, were determined by scanning transmission electron microscopy (STEM). Thin sections with thicknesses of approximately 100 nm were obtained by staining the samples with RuO<sub>4</sub> for 10 min, followed by cryo-microtomy using a Leica EM FC6. The sections were picked up on a lacey carbon coated copper grid (Electron Microscopy Sciences). STEM experiments were performed on a Tecnai F20 UT FEG, equipped with a high angle annular dark field (HAADF) detector, using 200 keV acceleration voltage, and atomic compositions were determined using a built-in energy-dispersive spectrometry (EDS) X-ray detector.

## 3. Results and discussion

The LiTFSI solubility limits in the liquid and solid electrolytes are reported in Table 1. The solubility limit ( $w_{\text{LiTFSI,limit}}$  in Table 1) is taken to be the average  $w_{\text{LiTFSI}}$  of the two solutions at the boundary between single-phase and two-phase systems. Based on the Flory-Huggins theory [43,44] often used to describe mixtures of small molecules and polymers, one expects the solubility of the small molecules to be reduced by crosslinking of the host polymer chains due to the increase in chain length and the concomitant reduction of entropy. The opposite is seen in Table 1. The solubility of LiTFSI in both types of solid electrolytes is higher than that in the liquid electrolytes. LiTFSI is more soluble in liquid POSS than in liquid PFPE. One expects this to affect the solubility of LiTFSI in the POSS-containing crosslinked solids. However, the fact that salt solubility is higher in the XL-POSS<sub>0.12</sub>-PFPE solids than either liquid is unexpected. Similarly, salt solubility in XL-PFPE is also higher than that of PFPE liquid. Perhaps the interactions between the salt ions and the crosslinked chains are fundamentally different from those in the liquid systems. Separate spectroscopic experiments that are beyond the scope of the present work may shed light on the factors that affect salt solubility in liquid and solid PFPEs. It is, perhaps, helpful to recall the processing steps involved in creating the solid electrolytes. In the XL-POSS<sub>0.12</sub>-PFPE case, the components are dissolved and reacted in THF at 70 °C. Similarly, XL-PFPE is made by dissolving the components at 90 °C. It is not surprising that the more LiTFSI is solubilized in the presence of solvent and elevated temperatures. The fact that salt did not precipitate after the solids were cooled to room temperature and dried (in the XL-POSS<sub>0.12</sub>-PFPE case) is surprising. We studied the crosslinked solids for several weeks after they were synthesized by examining them

**Table 1**  
Salt solubility in electrolytes.

Electrolyte	Liquid POSS	Liquid PFPE	Solid XL-POSS <sub>0.12</sub> -PFPE	Solid XL-PFPE
$w_{\text{LiTFSI,limit}}$	0.45	0.28	0.49	0.53
Highest $w_{\text{LiTFSI}}$ where homogeneous electrolyte is observed	0.4	0.25	0.47	0.5
Lowest $w_{\text{LiTFSI}}$ where heterogeneous electrolyte is observed	0.5	0.3	0.52	0.55

$w_{\text{LiTFSI}}$  is the weight fraction of LiTFSI.

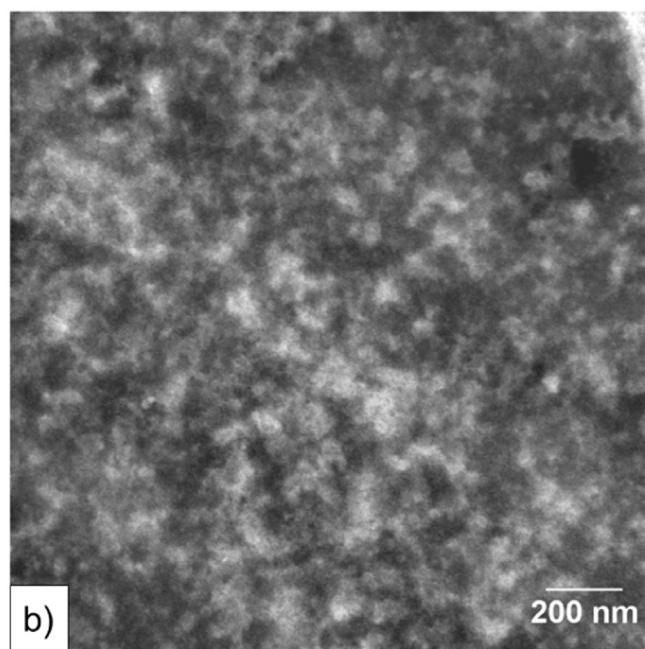
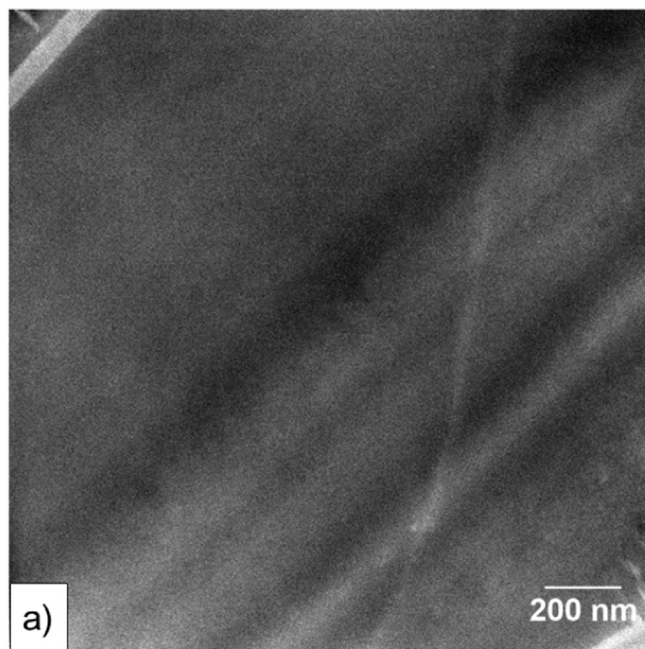


**Fig. 3.** STEM images of the solid electrolytes (a) XL-PFPE<sub>0.40</sub> and (b) XL-POSS<sub>0.12</sub>-PFPE<sub>0.35</sub>.

visually and by measuring the ionic conductivity. No evidence of salt precipitation was found. We also examined microtomed sections of the two classes of solid electrolytes by STEM to examine the possibility of the formation of small precipitates that cannot be seen visually. Typical micrographs of two crosslinked samples XL-PFPE<sub>0.40</sub> and XL-POSS<sub>0.13</sub>PFPE<sub>0.35</sub> are shown in Fig. 3a and b, respectively. These micrographs show no evidence of salt precipitation.

The STEM image of XL-PFPE<sub>0.40</sub> (Fig. 3a) is featureless, suggesting that the sample is homogeneous. The composition of this electrolyte was characterized by EDS to obtain the elemental maps of carbon, oxygen, fluorine, and sulfur. The result, shown in Fig. 4a, shows a uniform distribution of these elements throughout the samples. The absence of large sulfur rich domains indicates that the salt is uniformly distributed in the electrolyte; sulfur is only present in the TFSI<sup>-</sup> anion.

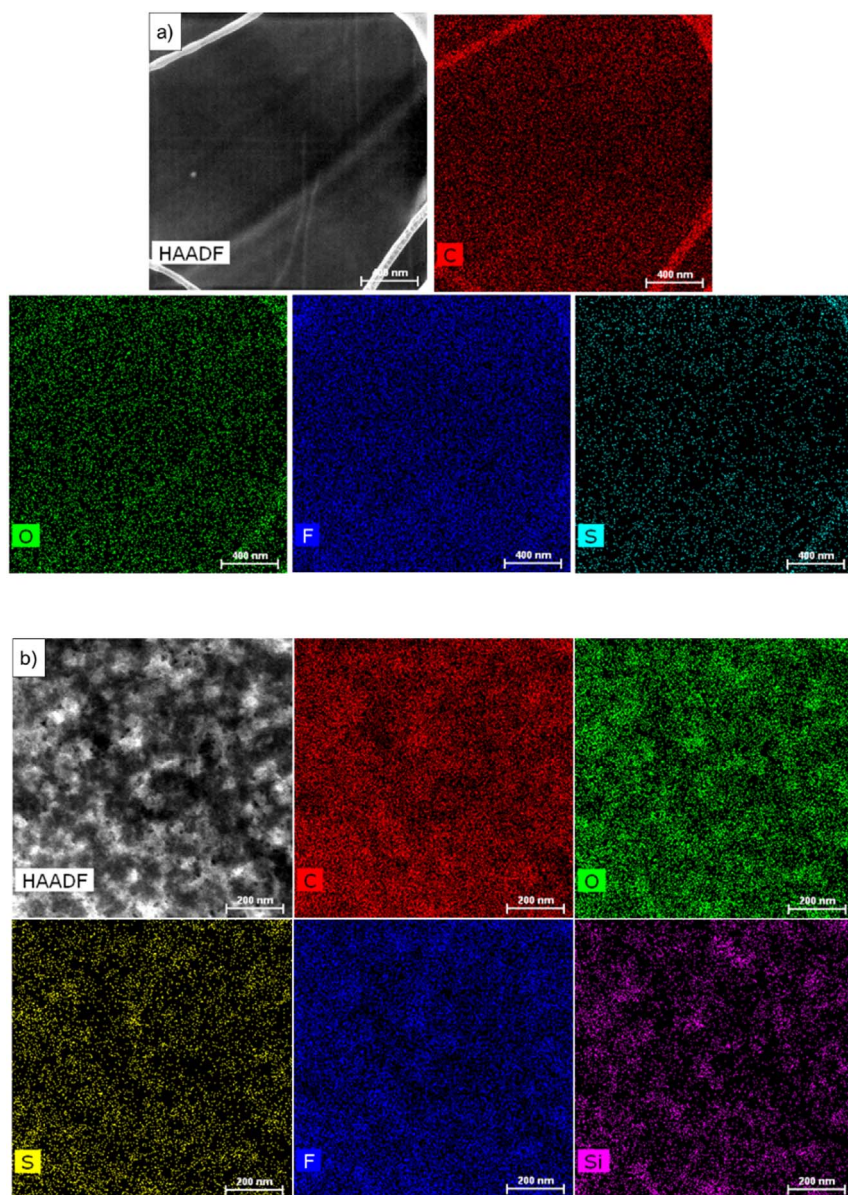


Fig. 4. EDS elemental maps of solid electrolytes (a) XL-PFPE\_0.40 and (b) XL-POSS<sub>0.12</sub>-PFPE\_0.35.

STEM image of XL-POSS<sub>0.12</sub>-PFPE\_0.35 shows some heterogeneity (Fig. 3b). The corresponding EDS map of this sample, shown in Fig. 4b, indicates the presence of PFPE-rich (dark) and POSS-rich (bright) domains: carbon, oxygen and fluorine elements are homogeneously distributed throughout the sample while silicon is concentrated in the bright domains. In addition, sulfur, which indicates the location of TFSI<sup>-</sup> anions, is seen in the dark PFPE domains, suggesting that the salt is primarily solvated by the fluorinated PFPE chains.

Representative DSC heating scans (heat flow versus temperature) are presented for XL-POSS<sub>0.12</sub>-PFPE\_0.26 and XL-PFPE\_0.25 in Fig. 5a. Also shown in Fig. 5a are representative data obtained from two liquid electrolytes, POSS\_0.10, PFPE\_0.10. All samples, except XL-PFPE\_0.25, exhibit signatures of a glass transition, and the  $T_g$ s of the samples are indicated by arrows on the DSC curves. The glass transition temperature associated with the motion of the fluorine atoms in pure PFPE liquids occurs at  $-90$  °C, a value that is outside the range of the instrument that we have access to [45]. The glass transition seen between  $-40$  and  $-60$  °C obtained from liquid PFPE\_0.10 may reflect the motion of the urethane methacrylate end-groups. At the same  $w_{\text{LiTFSI}}$  value, the POSS\_0.10 electrolyte presents a glass transition between  $-35$  and  $-60$  °C. The glass transition of XL-POSS<sub>0.12</sub>-PFPE\_0.26, is located

between  $-40$  and  $-10$  °C, a value that is higher than that of the liquid-based electrolyte at the same  $w_{\text{LiTFSI}}$ . For reasons that are not clear, none of the UV cured crosslinked solid electrolytes presented signatures of a glass transition.

The DSC data are summarized in Fig. 5b where  $T_g$  is plotted against  $w_{\text{LiTFSI}}$  for the three systems that showed glass transitions. In the neat state ( $w_{\text{LiTFSI}} = 0$ ), the solid XL-POSS<sub>0.12</sub>-PFPE presents the highest  $T_g$ , followed by POSS, followed by PFPE. At  $w_{\text{LiTFSI}} = 0.2$ , the  $T_g$  of the solid electrolyte is much higher than that of the liquid electrolytes. However, the increase in  $T_g$  with salt concentration from  $w_{\text{LiTFSI}}$  from 0.2 to 0.5 is weaker in the solid relative to the liquid electrolytes. This result is in agreement with those reported by Le Nest et al. in which it was shown that LiTFSI concentration has little influence on the glass transition temperature of crosslinked PEO-based networks [10]. All of the electrolytes exhibit similar  $T_g$ s in the vicinity of  $w_{\text{LiTFSI}} = 0.5$ . The observed linear relationships between  $T_g$  and  $w_{\text{LiTFSI}}$  in Fig. 5b are similar to those reported for PEO homopolymer and PEO-terminated POSS electrolytes [8,10,29,31]. For  $w_{\text{LiTFSI}} > 0.15$ , the POSS- and PFPE-based liquid electrolyte  $T_g$ s are similar.

The thermal stability of the solid electrolytes was investigated by TGA experiments. In Fig. 6a, the TGA curves of two representative

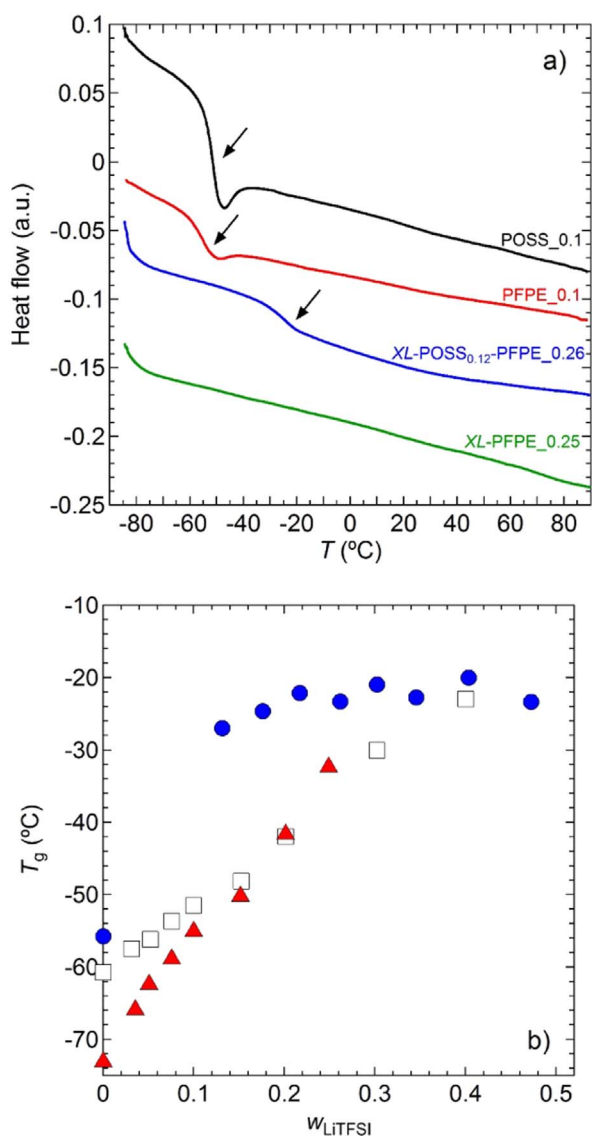


Fig. 5. (a) DSC thermograms, heat flow as a function of temperature, for selected electrolytes. The curves are shifted vertically by factors of 0.18, 0.12, 0.02, and 0 for POSS<sub>0.10</sub>, PFPE<sub>0.10</sub>, XL-POSS<sub>0.12</sub>-PFPE<sub>0.26</sub>, and XL-PFPE<sub>0.25</sub>, respectively. The heat flow is shown with exothermic peaks up. (b) Glass transition temperature as a function of the LiTFSI weight fraction for the (□) POSS, (▲) PFPE, and (●) XL-POSS<sub>0.12</sub>-PFPE electrolytes.

electrolytes, XL-POSS<sub>0.12</sub>-PFPE and XL-PFPE, at  $w_{\text{LiTFSI}}$  of 0.30 are shown. Both electrolytes are stable up to 260 °C with an onset temperature of electrolyte degradation ( $T_d$ ) at 268 °C and at 262 °C for the XL-PFPE<sub>0.30</sub> and XL-POSS<sub>0.12</sub>-PFPE<sub>0.30</sub>, respectively. An additional degradation event starting at about 330 °C is also seen for both electrolytes. This is attributed to LiTFSI degradation. In Fig. 6b, the  $T_d$  values of the two solid electrolytes, XL-PFPE and XL-POSS<sub>0.12</sub>-PFPE, are shown as a function of  $w_{\text{LiTFSI}}$ . Without Li salt,  $T_d$  is very similar for both materials, XL-PFPE<sub>0</sub> and XL-POSS<sub>0.12</sub>-PFPE<sub>0</sub>, with a value around 230 °C. For the XL-POSS<sub>0.12</sub>-PFPE electrolytes,  $T_d$  is almost independent of  $w_{\text{LiTFSI}}$  with an average value of  $258 \pm 4$  °C. More complex behavior is seen in the case of XL-PFPE. The excellent thermal stability of the electrolytes may prove important for Li polymer battery applications.

The ionic conductivity ( $\sigma$ ) of the liquid- and solid-based electrolytes was determined as a function of the temperature in between 30 and 90 °C. All of the electrolytes are above their glass transition temperatures in this regime. Fig. 7a shows  $\sigma$  of POSS, PFPE, XL-POSS<sub>0.12</sub>-PFPE, and XL-PFPE electrolytes at  $w_{\text{LiTFSI}} = 0.30$  as a function of  $1000/T$ .

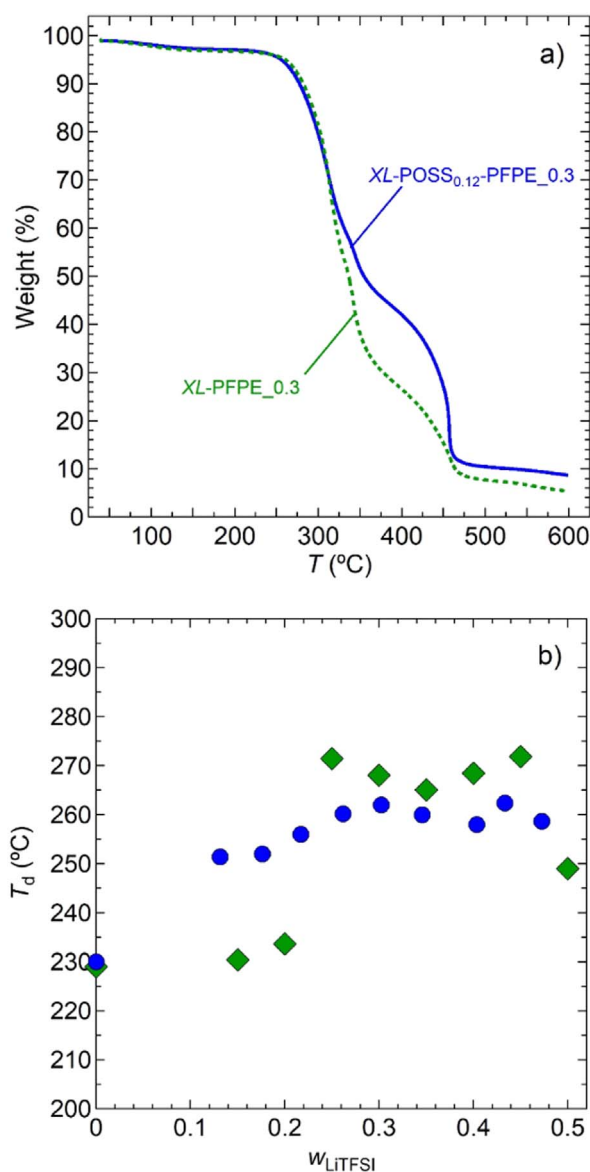


Fig. 6. (a) Thermogravimetric curves, weight percent as a function of the temperature for the XL-POSS<sub>0.12</sub>-PFPE<sub>0.30</sub> and XL-PFPE<sub>0.30</sub>. (b) Onset temperature of electrolyte degradation as a function of the LiTFSI weight fraction for the (●) XL-POSS<sub>0.12</sub>-PFPE and (◆) XL-PFPE electrolytes.

The conductivity of PFPE with urethane methacrylate end-groups is similar to that of other PFPE electrolytes reported in previous studies [37–41]. The conductivity of POSS<sub>0.30</sub> (the most conductive electrolyte in this study) is higher than that of the PFPE electrolyte by a factor  $3.2 \pm 0.8$  over the entire temperature window, reaching  $6.7 \times 10^{-5}$  S/cm at 90 °C. The ion-conducting capability of acrylopropyl-terminated POSS has not been reported previously; the reported work on ion-conducting POSS-containing systems is based on PEO-terminated POSS mixed with Li salt [29,46] and POSS-based ionic liquid electrolytes [47]. Not surprisingly, the conductivity of XL-POSS<sub>0.12</sub>-PFPE<sub>0.30</sub> is lower than that of liquid POSS<sub>0.30</sub> and PFPE<sub>0.30</sub> electrolytes (Fig. 7a). On average,  $\sigma$  of POSS<sub>0.30</sub> and PFPE<sub>0.30</sub> is higher than that of XL-POSS<sub>0.12</sub>-PFPE<sub>0.30</sub> by factors of  $16.4 \pm 6.4$  and  $4.7 \pm 0.9$ , respectively. The XL-PFPE electrolyte at  $w_{\text{LiTFSI}}$  of 0.30 is lower in conductivity than the other liquid- and solid-based PFPE electrolytes, reaching only  $1.1 \times 10^{-6}$  S/cm at 90 °C. The conductivity of XL-POSS<sub>0.12</sub>-PFPE<sub>0.30</sub> is larger than that of XL-PFPE<sub>0.30</sub> by factors ranging from 10 to 100. It is evident that the method used for crosslinking has a large effect on ionic conductivity. It

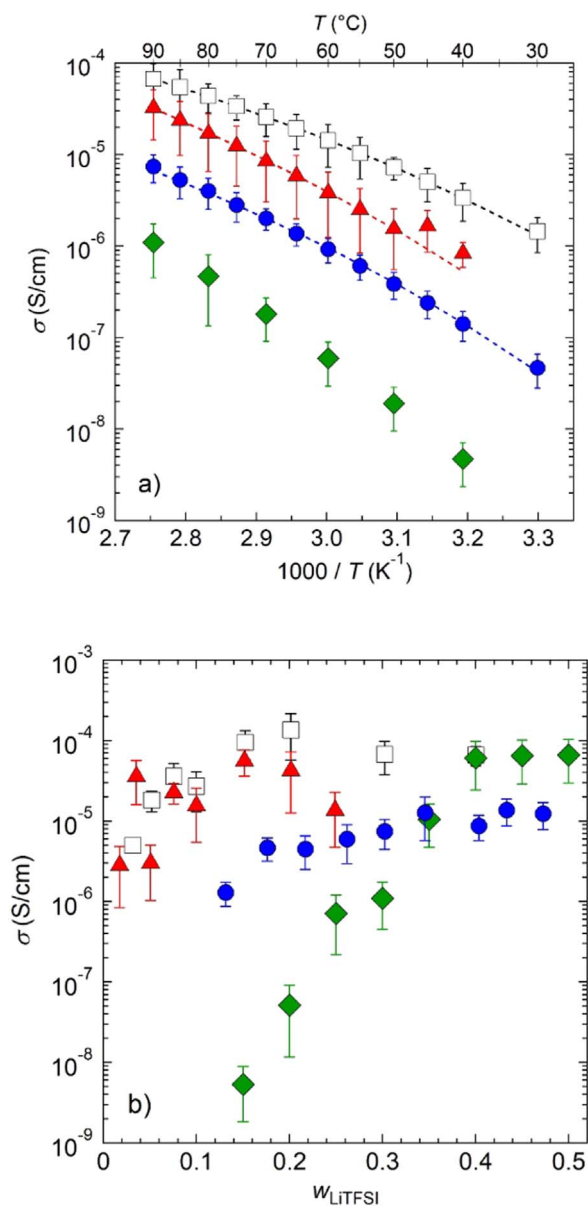


Fig. 7. (a) Ionic conductivity as a function of  $1000/T$  for each electrolyte at a LiTFSI weight fraction of 0.30. The dotted curves are the VTF fits using Eq. (2). (b) Ionic conductivity at 90 °C as a function of LiTFSI weight fraction. The symbols correspond to (□) POSS, (▲) PFPE, (●) XL-POSS<sub>0.12</sub>-PFPE, and (◆) XL-PFPE electrolytes.

is conceivable that the presence of POSS units in the crosslinks is responsible for the higher conductivity of XL-POSS<sub>0.12</sub>-PFPE<sub>0.30</sub> seen in Fig. 7a.

In Fig. 7b,  $\sigma$  is reported as a function of  $w_{\text{LiTFSI}}$  at 90 °C for the four electrolytes. For the liquid-based POSS electrolyte, the conductivity increases with LiTFSI content until a maximum at  $1.4 \times 10^{-4}$  S/cm for  $w_{\text{LiTFSI}} = 0.20$ . At higher  $w_{\text{LiTFSI}}$  values,  $\sigma$  decreases down to  $3.6 \times 10^{-5}$  S/cm at  $w_{\text{LiTFSI}} = 0.50$ , the solubility limit of LiTFSI in acrylopropyl-terminated POSS (see Table 1). This  $\sigma$ - $w_{\text{LiTFSI}}$  relationship is similar to that obtained in PEO and PEO-terminated POSS electrolytes with LiTFSI salt mixed in [8,29]. The  $\sigma$ - $w_{\text{LiTFSI}}$  data of the liquid PFPE electrolyte appears to be more complex with multiple local maxima. It is not clear if this is due to complex interactions between the salt and the solvent or experimental difficulties. There is, however, a general trend toward higher conductivity with increasing salt concentration, similar to that reported in previous studies on PFPE electrolytes [37,41]. In the solid electrolytes, XL-PFPE and XL-POSS<sub>0.12</sub>-PFPE,  $\sigma$

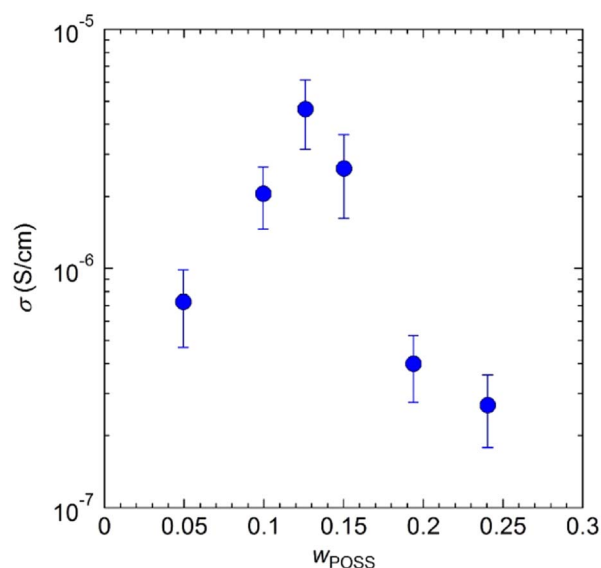


Fig. 8. Ionic conductivity at 90 °C as a function of the POSS weight fraction of the XL-POSS<sub>w</sub>POSS-PFPE<sub>0.17</sub> electrolytes.

increases with  $w_{\text{LiTFSI}}$ , reaching a plateau in the high salt concentration limit. For XL-POSS<sub>0.12</sub>-PFPE electrolytes  $\sigma = 1.3 \times 10^{-6}$  S/cm at  $w_{\text{LiTFSI}} = 0.13$ , and it reaches a plateau of  $1.2 \pm 0.2 \times 10^{-5}$  S/cm for  $w_{\text{LiTFSI}} > 0.34$ . For the XL-PFPE electrolytes,  $\sigma = 5.3 \times 10^{-9}$  S/cm for  $w_{\text{LiTFSI}} = 0.15$ , a value that is 3 orders of magnitude smaller than that of the POSS-based solid at similar salt loading, but reaches a plateau of  $6.5 \pm 0.2 \times 10^{-5}$  S/cm for  $w_{\text{LiTFSI}} \geq 0.40$ , a value that is higher than that of the POSS-based electrolyte by a factor of 5. It appears that the presence of POSS is important for conductivity in solid PFPEs with low salt loading. At high salt loading, the presence of POSS results in lower conductivity.

One expects the conductivity of thermally crosslinked solid PFPE electrolytes to depend on POSS loading. This dependence is shown in Fig. 8 where the conductivity of a series of solid electrolytes with  $w_{\text{LiTFSI}}$  held fixed at 0.17 is shown as a function of POSS weight fraction at 90 °C. We find a conductivity maximum at  $w_{\text{POSS}} = 0.12$ . Most of our work on this class of solid electrolytes was thus done on systems with  $w_{\text{POSS}} = 0.12$ .

Returning to Fig. 7a, the conductivities of all the reported electrolytes are consistent with the empirical Vogel–Tamman–Fulcher equation [48–50].

$$\sigma(T) = \frac{A}{\sqrt{T}} \cdot \exp\left(\frac{-B}{R \cdot (T - T_0)}\right) \quad (2)$$

where  $R$  is the gas constant,  $T_0$  is the glass transition temperature ( $T_g$ ) minus 50 K [51]. The conductivity data were fit using Eq. (2) using the pre-exponential parameter,  $A$ , and the activation energy,  $B$ , as free parameters, while  $T_0$  was fixed using the electrolyte  $T_g$  values obtained from DSC (Fig. 5b). We exclude the XL-PFPE electrolytes from this discussion as we were unable to detect a signature of the glass transition in DSC. The curves in Fig. 7a represent VTF fits through the data from the other three electrolytes.

In addition to  $T_g$ , the conductivity of our electrolytes is affected by factors such as ion dissociation and mobility of the solvent molecules. One can factor out the effect of  $T_g$  by examining the dependence of conductivity as a function of  $1000 / (T - T_g + 50)$  as suggested by the VTF equation. This is shown in Fig. 9. At low salt loading ( $w_{\text{LiTFSI}} = 0.11$ ), the liquid conductivities are about an order of magnitude above that of the POSS-based solid (XL-POSS<sub>0.12</sub>-PFPE) electrolyte (Fig. 9a). The data obtained from the three systems appear to be parallel lines when plotted in the VTF format, suggesting that the main difference between the electrolytes is in the parameter  $A$  (not  $B$ ). It is

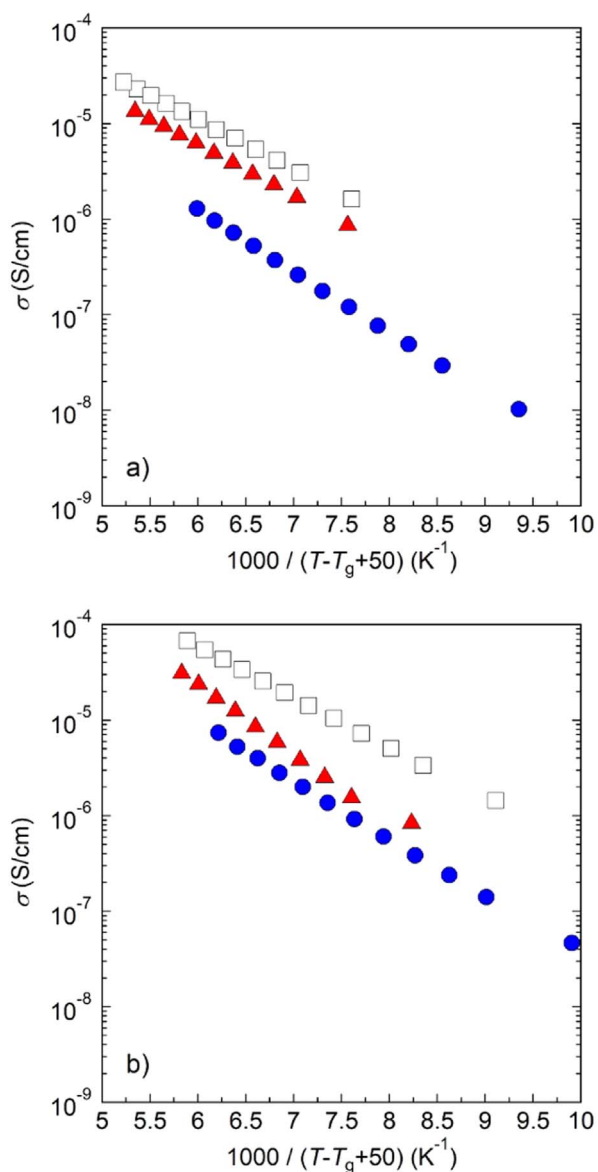


Fig. 9. (a) Ionic conductivity as a function of  $1000 / (T - T_g + 50)$  for the (□) POSS<sub>0.1</sub>, (▲) PFPE<sub>0.1</sub>, and (●) XL-POSS<sub>0.12</sub>-PFPE<sub>0.13</sub> electrolytes. (b) Ionic conductivity as a function of  $1000 / (T - T_g + 50)$  for the (□) POSS<sub>0.3</sub>, (▲) PFPE<sub>0.3</sub>, and (●) XL-POSS<sub>0.12</sub>-PFPE<sub>0.3</sub> electrolytes.

generally assumed that  $A$  reflects the concentration of effective charge carriers and thus the data in Fig. 9a suggests that more ion pairs are present in the solid electrolyte with  $w_{\text{LiTFSI}} = 0.11$ . At high salt loading ( $w_{\text{LiTFSI}} = 0.30$ ), the distinction between the solids and liquids is diminished, as shown in Fig. 9b, suggesting that the concentration of effective charge carriers in the liquids and solids is similar.

The VTF parameters obtained from our electrolytes are summarized in Fig. 10 where the dependencies of  $A$  and  $B$  on  $w_{\text{LiTFSI}}$  are shown. As seen in Fig. 10a,  $A$  is a strong function of the nature of the solvent (solid versus liquid). In addition,  $A$  increases by two orders of magnitude over the accessible salt concentration range. In contrast,  $B$  is not a strong function of either the nature of the solvent nor salt concentration (Fig. 10b), increasing by a modest factor of 1.7 over the accessible salt concentration range.

#### 4. Conclusion

We report on the first attempt to synthesize solid fluorinated

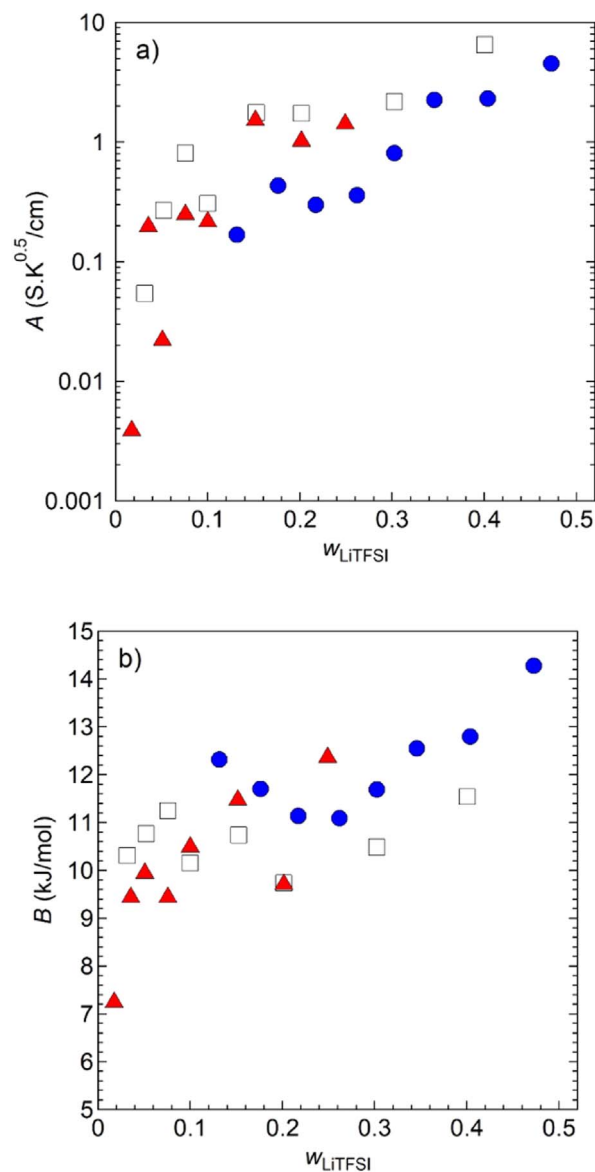


Fig. 10. VTF parameters, (a)  $A$  and (b)  $B$ , obtained using Eq. (2) as a function of LiTFSI weight fraction. The symbols correspond to (□) POSS, (▲) PFPE, and (●) XL-POSS<sub>0.12</sub>-PFPE electrolytes.

electrolytes using PFPE with urethane methacrylate end-groups. Two kinds of crosslinked systems were prepared using thermally and UV activated curing reactions. For the thermally crosslinked electrolytes, POSS nanoparticles with acrylopropyl groups were used as the cross-linking agent. The UV cured electrolytes were prepared using a photoinitiator. In both cases, LiTFSI salt was mixed into the uncured liquid prior to the crosslinking step. We compared the ionic conductivity of solid electrolytes with that of the two liquid precursors in our systems: PFPE with urethane methacrylate end-groups and POSS with acrylopropyl groups, both mixed with LiTFSI. To our surprise, mixtures of POSS and LiTFSI exhibited significant ionic conductivity. (The conductivity of the liquid PFPE electrolyte was similar to that reported in previous studies [37,41].) The LiTFSI solubility limit in both types of solid electrolytes is higher than that of the liquid electrolytes. After synthesis, no evidence of salt precipitation was found for several weeks. In addition, LiTFSI is more soluble in liquid POSS than in liquid PFPE. Glass transition temperatures were detected by DSC for the liquid-based and thermally crosslinked solid electrolytes. None of the UV crosslinked solid electrolytes presented signatures of a glass transition. Upon

addition of LiTFSI, the increase in  $T_g$  with  $w_{\text{LiTFSI}}$  from 0.2 to 0.5 is weaker in the solid relative to the liquid electrolytes. A general trend is seen toward higher conductivity with increasing salt concentration. For the solid electrolytes, XL-PFPE and XL-POSS<sub>0.12</sub>-PFPE,  $\sigma$  increases with  $w_{\text{LiTFSI}}$  reaching a plateau in the high salt concentration limit. At the lowest salt concentration studied, the conductivity of the POSS-containing solid is greater than that of the solid that does not contain POSS by a factor of 243. It appears as though the salt ions selectively interact with the POSS moieties at low salt loadings and that this increases salt dissociation. Our conductivity measurements on liquid mixtures of POSS and LiTFSI provide some support for this. At high salt loading, however, the conductivity of the POSS-containing solid and that of the solid that does not contain POSS is within a factor of 5, and the conductivity of the latter solid is higher. We posit that the conductivity in the high concentration limit is dominated by the interactions between salt and PFPE chains. It is evident that in addition to  $T_g$ , the conductivity of the electrolytes is affected by ion dissociation and mobility of the solvent molecules. We used the VTF framework to quantify these factors. The VTF prefactor,  $A$ , that is related to the concentration of effective charge carriers, is a strong function of the nature of the solvent (solid versus liquid) whereas the activation energy,  $B$ , is neither a strong function of the nature of the solvent nor salt concentration.

We hope that the present work sets the stage for developing solid fluorinated polymer electrolytes with optimized properties.

## Acknowledgements

This project is primarily funded by the National Science Foundation, Grant Number 1505669, under the SusChEM initiative. Irune Villaluenga and Mahesh Bhatt were supported by the Joint Center for Energy Storage Research, an Energy Innovation Hub funded by the U.S. Department of Energy (DOE), Office of Science, Basic Energy Sciences (BES). Didier Devaux was supported by a postdoctoral fellowship from the Philomathia Center at the University of California at Berkeley.

## References

- J.-M. Tarascon, M. Armand, Issues and challenges facing rechargeable lithium batteries, *Nature* 414 (2001) 359–367.
- M. Armand, The history of polymer electrolytes, *Solid State Ionics* 69 (1994) 309–319.
- D.E. Fenton, J.M. Parker, P.V. Wright, Complexes of alkali metal ions with poly(ethylene oxide), *Polymer* 14 (1973) 589.
- M. Armand, J.M. Chabagno, M.J. Duclot, No title, in: V. Fast Ion Transport in Solids Electrodes and Electrolytes P. Vashishta, Mundy, J.-N. & Shenoy, G. K. (Ed.), North-Holland, Amsterdam, n.d.
- M. Doyle, T.F. Fuller, J. Newman, The importance of the lithium ion transference number in lithium/polymer cells, *Electrochim. Acta* 39 (1994) 2073–2081.
- M. Doyle, J. Newman, Analysis of transference number measurements based on the potentiostatic polarization of solid polymer electrolytes, *J. Electrochem. Soc.* 142 (1995) 3465–3468.
- J. Shi, C.A. Vincent, The effect of molecular-weight on cation mobility in polymer electrolytes, *Solid State Ionics* 60 (1993) 11–17.
- S. Lascaud, M. Perrier, A. Vallée, S. Besner, J. Prudhomme, M. Armand, Phase diagrams and conductivity behavior of poly(ethylene oxide) molten-salt rubbery electrolytes, *Macromolecules* 27 (1994) 7469–7477.
- A. Killis, J.F. Le Nest, A. Gandini, H. Cheradame, J.P. Cohen-Addad, Correlation among transport properties in ionically conducting cross-linked networks, *Solid State Ionics* 14 (1984) 231–237.
- J.F. Le Nest, S. Callens, A. Gandini, M. Armand, A new polymer network for ionic-conduction, *Electrochim. Acta* 37 (1992) 1585–1588.
- F. Alloin, J.Y. Sanchez, M. Armand, Electrochemical behavior of lithium electrolytes based on new polyether networks, *J. Electrochem. Soc.* 141 (1994) 1915–1920.
- M. Watanabe, A. Nishimoto, Effects of network structures and incorporated salt species on electrochemical properties of polyether-based polymer electrolytes, *Solid State Ionics* 79 (1995) 306–312.
- M.C. Borghini, M. Mastragostino, A. Zanelli, Reliability of lithium batteries with crosslinked polymer electrolytes, *Electrochim. Acta* 41 (1996) 2369.
- B. Laik, L. Legrand, A. Chausse, R. Messina, Ion-ion interactions and lithium stability in a crosslinked PEO containing lithium salts, *Electrochim. Acta* 44 (1998) 773–780.
- M. Kono, E. Hayashi, M. Watanabe, Network polymer electrolytes with free chain ends as internal plasticizer, *J. Electrochem. Soc.* 145 (1998) 1521–1527.
- J.F. Snyder, R.H. Carter, E.D. Wetzel, Electrochemical and mechanical behavior in mechanically robust solid polymer electrolytes for use in multifunctional structural batteries, *Chem. Mater.* 19 (2007) 3793–3801.
- R. Khurana, J.L. Schaefer, L.A. Archer, G.W. Coates, Suppression of lithium dendrite growth using cross-linked polyethylene/poly(ethylene oxide) electrolytes: a new approach for practical lithium-metal polymer batteries, *J. Am. Chem. Soc.* 136 (2014) 7395–7402.
- Z. Xue, D. He, X. Xie, Poly(ethylene oxide)-based electrolytes for lithium-ion batteries, *J. Mater. Chem. A* 3 (2015) 19218–19253.
- Q. Pan, D.M. Smith, H. Qi, S. Wang, C.Y. Li, Hybrid electrolytes with controlled network structures for lithium metal batteries, *Adv. Mater.* 27 (2015) 5995–6001.
- J.Y. Lee, Y.M. Lee, B. Bhattacharya, Y.-C. Nho, J.-K. Park, Solid polymer electrolytes based on crosslinkable polyoctahedral silsesquioxanes (POSS) for room temperature lithium polymer batteries, *J. Solid State Electrochem.* 14 (2010) 1445–1449.
- B.K. Lee, N.-G. Cha, L.-Y. Hong, D.-P. Kim, H. Tanaka, H.Y. Lee, T. Kawa, Photocurable silsesquioxane-based formulations as versatile resins for nanoimprint lithography, *Langmuir* 26 (2010) 14915–14922.
- F.B. Dias, L. Plomp, J.B.J. Veldhuis, Trends in polymer electrolytes for secondary lithium batteries, *J. Power Sources* 88 (2000) 169–191.
- D. Devaux, R. Bouchet, D. Glé, R. Denoyel, Mechanism of ion transport in PEO/LiTFSI complexes: effect of temperature, molecular weight and end groups, *Solid State Ionics* 227 (2012) 119–127.
- G. Li, L. Wang, H. Ni, C.U. Pittman Jr., Polyhedral oligomeric silsesquioxane (POSS) polymers and copolymers: a review, *J. Inorg. Organomet. Polym.* 11 (2002) 123–154.
- S.-W. Kuo, F.-C. Chang, POSS related polymer nanocomposites, *Prog. Polym. Sci.* 36 (2011) 1649–1696.
- D.B. Cordes, P.D. Lickiss, F. Rataboul, Recent developments in the chemistry of cubic polyhedral oligosilsesquioxanes, *Chem. Rev.* 110 (2010) 2081–2173.
- P. Maitra, S.L. Wunder, Oligomeric poly(ethylene oxide)-functionalized silsesquioxanes: interfacial effects on  $T_g$ ,  $T_m$ , and  $\Delta H_m$ , *Chem. Mater.* 14 (2002) 4494–4497.
- P. Maitra, S.L. Wunder, POSS based electrolytes for rechargeable lithium batteries, *Electrochem. Solid-State Lett.* 7 (2004) A88–A92.
- H. Zhang, S. Kulkarni, S.L. Wunder, Polyethylene glycol functionalized polyoctahedral silsesquioxanes as electrolytes for lithium batteries, *J. Electrochem. Soc.* 253 (2006) A239–A248.
- H. Zhang, S. Kulkarni, S.L. Wunder, Blends of POSS – PEO( $n = 4$ )8 and high molecular weight poly(ethylene oxide) as solid polymer electrolytes for lithium batteries, *J. Phys. Chem. B* 111 (2007) 3583–3590.
- P.R. Chinnam, S.L. Wunder, Polyoctahedral silsesquioxane-nanoparticle electrolytes for lithium batteries: POSS-lithium salts and POSS-PEGs, *Chem. Mater.* 23 (2011) 5111–5121.
- P.R. Chinnam, S.L. Wunder, Self-assembled Janus-like multi-ionic lithium salts form nano-structured solid polymer electrolytes with high ionic conductivity and Li<sup>+</sup> ion transference number, *J. Mater. Chem. A* 1 (2013) 1731–1739.
- F. Croce, G.B. Appetechi, L. Persi, B. Scrosati, Nanocomposite polymer electrolytes for lithium batteries, *Nature* 394 (1998) 456–458.
- P. Johansson, M.A. Ratner, D.F. Shriver, The influence of inert oxide fillers on poly(ethylene oxide) and amorphous poly(ethylene oxide) based polymer electrolytes, *J. Phys. Chem. B* 105 (2001) 9016–9021.
- M.A. Webb, Y. Jung, D.M. Pesko, B.M. Savoie, U. Yamamoto, G.W. Coates, N.P. Balsara, Z.-G. Wang, T.F. Miller, Systematic computational and experimental investigation of lithium-ion transport mechanisms in polyester-based polymer electrolytes, *ACS Cent. Sci.* 1 (2015) 198–205.
- M. Chintapalli, T.N.P. Le, N.R. Venkatesan, N.G. Mackay, A.A. Rojas, J.L. Thelen, X.C. Chen, D. Devaux, N.P. Balsara, Structure and ionic conductivity of polystyrene-block-poly(ethylene oxide) electrolytes in the high salt concentration limit, *Macromolecules* 49 (2016) 1770–1780.
- D.H.C. Wong, J.L. Thelen, Y. Fu, D. Devaux, A.A. Pandya, V.S. Battaglia, N.P. Balsara, J.M. DeSimone, Nonflammable perfluoropolyether-based electrolytes for lithium batteries, *Proc. Natl. Acad. Sci. U. S. A.* 111 (2014) 3327–3331.
- D.H.C. Wong, A. Vitale, D. Devaux, A. Taylor, A.A. Pandya, D.T. Hallinan, J.L. Thelen, S.J. Mecham, A.M. Lapidus, P.R. Resnick, T.J. Meyer, R.M. Kostecki, N.P. Balsara, J.M. DeSimone, Phase behavior and electrochemical characterization of blends of perfluoropolyether, poly(ethylene glycol), and a lithium salt, *Chem. Mater.* 27 (2015) 597–603.
- D. Devaux, Y.H. Chang, I. Villaluenga, X.C. Chen, M. Chintapalli, J.M. DeSimone, N.P. Balsara, Conductivity of carbonate- and perfluoropolyether-based electrolytes in porous separators, *J. Power Sources* 323 (2016) 158–165.
- M. Chintapalli, K. Timachova, K.R. Olson, S.J. Mecham, D. Devaux, J.M. DeSimone, N.P. Balsara, Relationship between conductivity, ion diffusion, and transference number in perfluoropolyether electrolytes, *Macromolecules* 49 (2016) 3508–3515.
- K.R. Olson, D.H.C. Wong, M. Chintapalli, K. Timachova, R. Januszewicz, W.F.M. Daniel, S. Mecham, S. Sheiko, N.P. Balsara, J.M. DeSimone, Liquid perfluoropolyether electrolytes with enhanced ionic conductivity for lithium battery applications, *Polymer* 100 (2016) 126–133.
- S.S. Williams, S. Retterer, R. Lopez, R. Ruiz, E.T. Samulski, J.M. DeSimone, High-resolution PFPE-based molding techniques for nanofabrication of high-pattern density, sub-20 nm features: a fundamental materials approach, *Nano Lett.* 10 (2010) 1421–1428.
- M.L. Huggins, Solutions of long chain compounds, *J. Chem. Phys.* 9 (1941) 440.
- P.J. Flory, Thermodynamics of high polymer solutions, *J. Chem. Phys.* 10 (1942) 51–61.
- Z. Hu, J.A. Finlay, L. Chen, D.E. Betts, M.A. Hillmyer, M.E. Callow, J.A. Callow, J.M. DeSimone, Photochemically cross-linked perfluoropolyether-based elastomers:

- synthesis, physical characterization, and biofouling evaluation, *Macromolecules* 42 (2009) 6999–7007.
- [46] D.-G. Kim, J. Shim, J.H. Lee, S.-J. Kwon, J.-H. Baik, J.-C. Lee, Preparation of solid-state composite electrolytes based on organic/inorganic hybrid star-shaped polymer and PEG-functionalized POSS for all-solid-state lithium battery applications, *Polymer* 54 (2013) 5812–5820.
- [47] K. Tanaka, F. Ishiguro, Y. Chujo, POSS ionic liquid, *J. Am. Chem. Soc.* 132 (2010) 17649–17651.
- [48] H. Vogel, The law of the relationship between viscosity of liquids and the temperature, *Phys. Z.* 22 (1921) 645–646.
- [49] V.G. Tamman, W. Hesse, Die Abhängigkeit der Viscosität von der Temperatur bei Unterkühlten Flüssigkeiten, *Z. Anorg. Allg. Chem.* 156 (1926) 245–257.
- [50] G.S. Fulcher, Analysis of recent measurements of the viscosity of glasses, *J. Am. Ceram. Soc.* 8 (1925) 339–355.
- [51] J.L. Souquet, M. Duclot, M. Levy, Salt-polymer complexes: strong or weak electrolytes? *Solid State Ionics* 85 (1996) 149–157.